

Improving the Simulation of Quark and Gluon Jets with Herwig 7

Daniel Reichelt^{a,1}, Peter Richardson^{b,2,3}, Andrzej Siodmok^{c,4}

¹Institut für Kern- und Teilchenphysik, Technische Universität Dresden

²Theory Department, CERN, Geneva

³IPPP, Department of Physics, Durham University

⁴The Henryk Niewodniczański Institute of Nuclear Physics in Cracow, Polish Academy of Sciences

Received: date / Accepted: date

Abstract The properties of quark and gluon jets, and the differences between them, are increasingly important at the LHC. However, Monte Carlo event generators are normally tuned to data from e^+e^- collisions which are primarily sensitive to quark-initiated jets. In order to improve the description of gluon jets we make improvements to the perturbative and the non-perturbative modelling of gluon jets and include data with gluon-initiated jets in the tuning for the first time. The resultant tunes significantly improve the description of gluon jets and are now the default in Herwig 7.1.

1 Introduction

Monte Carlo generators are essential tools, both for the design of future experiments and the analysis of data from the LHC, and previous collider experiments. Modern event generators [1–3] provide a simulation of exclusive events based on the combination of fixed-order perturbative results, resummation of large logarithms of scales using the parton-shower approach and non-perturbative models of hadronization and multiple-parton scattering.¹

These simulations rely on universality and factorization in order to construct a simulation of the complex final states observed in hadronic collisions. This allows the simulation of final-state radiation in the parton shower and the non-perturbative hadronization models to be first developed, and the parameters of the the model tuned, using the simpler and cleaner environment of e^+e^- collisions, and then applied to more complicated hadronic collisions. These models are then combined with the parton-shower simulation of initial-state radiation, a multiple scattering model of the underlying

event and a non-perturbative colour reconnection model in order to describe hadronic collisions. In principle universality requires that the colour reconnection model is also used to describe leptonic collisions. In practice however colour reconnection has little effect on the distributions which so far have been used to develop and tune the models. These models are therefore usually either not included at all for the simulation of leptonic collisions, or if they are, the parameters are determined by tuning to hadronic data sensitive to multiple partonic scattering.

As the LHC accumulates data at an unprecedented rate there are a number of observables which are not well described by current Monte Carlo event generators, and where the limitations of this approach have started to become obvious, for example:

- the difference in the properties of jets initiated by quarks and gluons is not well described with generators predicting either a larger or smaller difference between the jets than is observed by the LHC experiments [5];
- the transverse momentum spectra of identified baryons and strange hadrons which are not well described by current generators. [6];
- long-range correlations in high multiplicity events [7, 8].

In this paper we will focus on improvements to the perturbative and non-perturbative modelling to give a better description of both quark- and gluon-initiated jets, as well as the differences between them in Herwig 7. Beyond leading order there is no clear distinction between quark and gluon jets and the definition will depend on the analysis.² As e^+e^- annihilation to hadrons starts with an initial partonic quark-antiquark configuration the data used to develop the final-state parton-shower algorithm, tune its parameters and those of the hadronization model, are dominated by quark-initiated jets. However at the LHC jets initiated by gluons

^ae-mail: daniel.reichelt@tu-dresden.de

^be-mail: peter.richardson@durham.ac.uk

^ce-mail: andrzej.siodmok@ifj.edu.pl

¹For a recent review of modern Monte Carlo event generators see [4].

²See Ref. [9] for a more detailed discussion.

can often dominate, depending on the production process, rapidity and transverse momentum of the jets. Regrettably while there is great interest in the differences between quark and gluon jets at the LHC most of the experimental studies have concentrated on differentiating between quark and gluon jets using neural network, or similar, techniques which makes a direct comparison with simulated hadron-level events impossible. We will therefore use some recent data from the ATLAS experiment [10] which is sensitive to both quark and gluon jet properties, together with data on gluon jets in e^+e^- collisions from the OPAL experiment [11, 12] which has not previously been used in the development and tuning of the current generation of Monte Carlo event generators to study the properties of gluon jets.

In the next section we will first recap the default parton-shower algorithm used in Herwig 7 focusing on recent changes we have made to improve the simulation of both quark and gluon jets. In Section 3 we will briefly review the important parameters in the cluster hadronization model used in Herwig 7 and identify the issues which may lead to different treatments of quark and gluon jets. We will then discuss the tuning strategy used to produce the tunes presented in this paper. We present our results in Section 5³ followed by our conclusions.

2 Herwig 7 Parton-Shower Algorithm

The default Herwig 7 parton-shower algorithm [13] is an improved angular-ordered parton shower. In this approach the momenta of the partons produced in the parton shower are decomposed in terms of the 4-momentum of the parton initiating the jet, p ($p^2 = m^2$, the *on-shell* parton mass-squared), a light-like reference vector, n , in the direction of the colour partner of the parton initiating the jet and the momentum transverse to the direction of p and n . The four momentum of any parton produced in the evolution of the jet can be decomposed as

$$q_i = \alpha_i p + \beta_i n + q_{\perp i}, \quad (1)$$

where α_i and β_i are coefficients and $q_{\perp i}$ is the transverse four momentum of the parton ($q_{\perp i} \cdot p = q_{\perp i} \cdot n = 0$).

If we consider the branching of a final-state parton i to two partons j and k , i.e. $i \rightarrow jk$ as shown in Fig. 1, the branching is described by the evolution variable

$$\tilde{q}_i^2 = \frac{q_i^2 - m_i^2}{z_i(1-z_i)}, \quad (2)$$

where q_i^2 is the square of the virtual mass developed by the parton i in the branching, m_i is the physical mass of parton i ,

³Additional results on quark and gluon jet discrimination power are included in the Appendix.

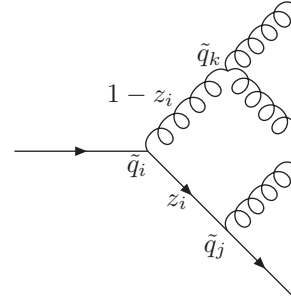


Fig. 1 Branching of the parton i to produce the partons j, k which then undergo subsequent branching.

and z_i is the momentum fraction of the parton j defined such that

$$\alpha_j = z_i \alpha_i, \quad \alpha_k = (1 - z_i) \alpha_i. \quad (3)$$

The transverse momenta of the partons produced in the branching are

$$q_{\perp j} = z_i q_{\perp i} + k_{\perp i} \quad q_{\perp k} = (1 - z_i) q_{\perp i} - k_{\perp i}, \quad (4)$$

where $k_{\perp i}$ is the transverse momentum generated in the branching. In this case the virtuality of the parton i is

$$q_i^2 = \frac{p_{T i}^2}{z(1-z)} + \frac{m_j^2}{z} + \frac{m_k^2}{1-z}, \quad (5)$$

where p_T is the magnitude of the transverse momentum produced in the branching defined such that $k_{\perp i}^2 = -p_{T i}^2$.

In this case the probability for a single branching to happen is

$$d\mathcal{P} = \frac{d\tilde{q}_i^2}{\tilde{q}_i^2} \frac{\alpha_S}{2\pi} \frac{d\phi_i}{2\pi} dz_i P_{i \rightarrow jk}(z, \tilde{q}), \quad (6)$$

where $P_{i \rightarrow jk}(z, \tilde{q})$ is the quasi-collinear splitting function, and ϕ_i is the azimuthal angle of the transverse momentum $k_{\perp i}$ generated in the splitting.

As the branching probability is singular for massless partons an infrared cut-off is required to regularise the singularity. In HERWIG 6 [14] and early versions of Herwig++ [15] the cut-off was implemented by giving the partons an infrared mass. However while this remains an option in later versions of Herwig++ and Herwig 7 [1] the default cut-off is now on the minimum transverse momentum of the branching [16].

In order to resum the dominant subleading logarithms [17] the transverse momentum of the branching is used as the scale for the strong coupling constant. This also means that the strong coupling used in the parton shower is that defined in the Catani-Marchesini-Webber (CMW) scheme which includes the subleading terms via a redefinition of QCD scale, Λ_{QCD} .

While this specifies both the branching probability and kinematics of the partons for a single emission in the case of subsequent emission from the daughter partons j and/or k we must decide which properties of the originally generated kinematics to preserve once the masses of j and/or k in Eqn. 5 are no longer the infrared cut-off masses but the virtualities generated by any subsequent emissions. While this choice is formally subleading it can have a large effect on physical observables.

In Herwig++ the transverse momentum of the branching was calculated using Eqn. 5 and the infrared cut-off masses when the emission was generated and then preserved during the subsequent evolution of the daughter partons. In Herwig 7.0 the default option was to instead preserve the virtuality of the branching and calculate the transverse momentum of the branching using the virtual masses the daughter partons develop due to subsequent emissions. This means that if the daughter partons develop large virtual masses the transverse momentum of the branching is reduced, and in some cases the branching has to be vetoed if there is no solution of Eqn. 5. However, this choice inhibits further soft emission and significantly changes the evolution by vetoing emissions and leads to incorrect evolution of observables. We therefore consider a further choice in which if it is possible to preserve the virtuality and still have a solution for $p_T^2 > 0$ we do so, however if this is not possible instead of vetoing the emission we set $p_T = 0$ and allow the virtuality to increase.

The most important parameters which affect the behaviour of the parton shower and which we will tune in this paper are:

- the choice of whether to preserve p_T or q^2 during the subsequent evolution;
- the value of the strong coupling constant **AlphaMZ**, taken to be $\alpha_s^{\text{CMW}}(M_Z)$, value of the coupling constant in the CMW scheme at the mass of the Z boson, M_Z ;
- the cut-off in the parton shower⁴. For a cut-off in p_T this is the minimum transverse momentum allowed for the branchings in the shower, p_T^{min} . For a virtuality cut-off we parameterize the threshold for different flavours as

$$Q_g = \max\left(\frac{\delta - am_q}{b}, c\right), \quad (7)$$

where a and b are parameters chosen to give a threshold which is slightly reduced for heavier quarks. The parameter $c = 0.3$ GeV is chosen to prevent the cutoff becoming too small, we also keep the default value of $b = 2.3$. Only the parameters δ (cutoffKinScale) and a (aParameter) are tuned to the data.

⁴There is an option to extend the parton-shower radiation to the non-perturbative region and effectively remove the cut-off, see [18].

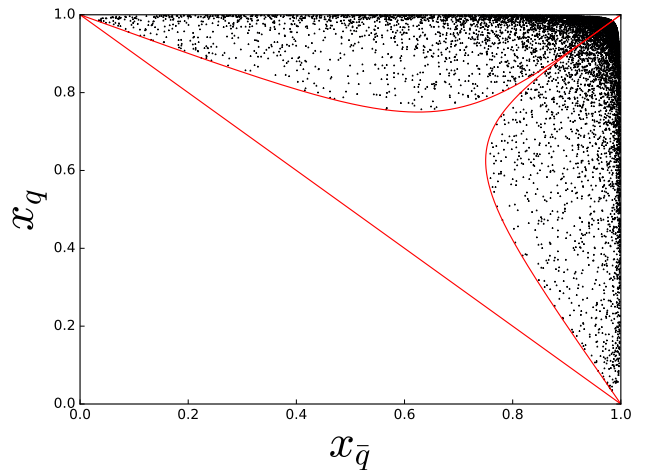


Fig. 2 Dalitz plot for $e^+e^- \rightarrow q\bar{q}g$ showing the region of phase space filled by one emission from the quark and antiquark in the angular-ordered parton shower. The line shows the limits for the parton-shower emission. $x_i = 2E_i/Q$ where E_i is the energy of parton i and Q is the centre-of-mass energy of the collision.

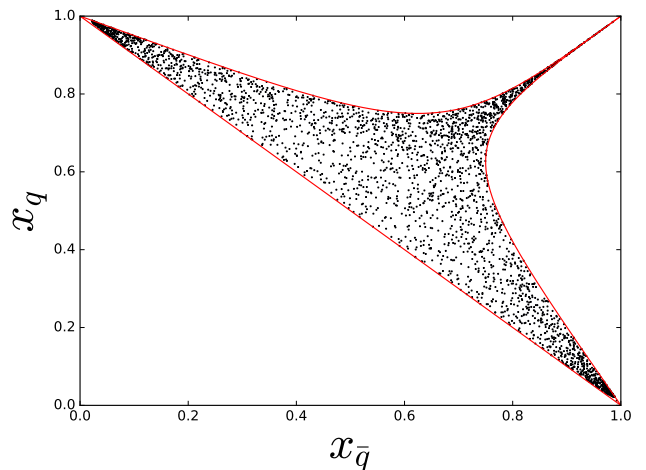


Fig. 3 Dalitz plot for $e^+e^- \rightarrow q\bar{q}g$ showing the emission from the hard matrix element correction into the *dead-zone* which is not populated by parton-shower emission. The line shows the limits for the parton-shower emission. $x_i = 2E_i/Q$ where E_i is the energy of parton i and Q is the centre-of-mass energy of the collision.

There is one other major feature of the angular-ordered parton shower which we need to consider. The angular ordering of the parton shower, which is used to implement the phenomenon of colour coherence, leads to regions of phase space in which there is no gluon emission. Consider for example the process $e^+e^- \rightarrow q\bar{q}g$. In this case there is a *dead-zone* which is not filled by one emission from the parton shower, as shown in Fig. 2. Given this deficit of hard, wide-angle emission it is necessary to combine the parton-shower with the fixed-order calculation of $e^+e^- \rightarrow q\bar{q}g$. There are

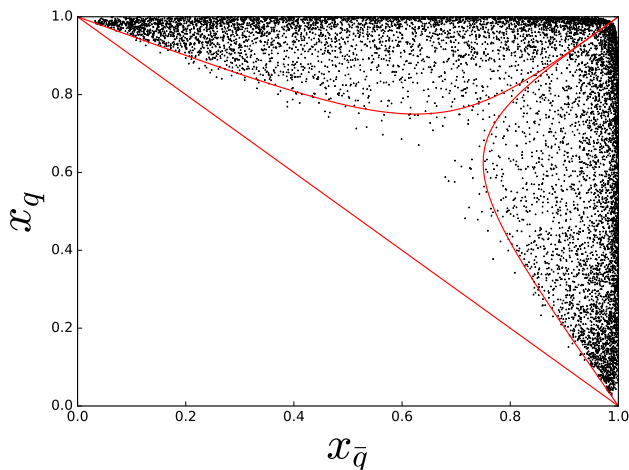


Fig. 4 Dalitz plot for $e^+e^- \rightarrow q\bar{q}$ showing the region of phase space filled after multiple emission from the quark and antiquark in the angular-ordered parton shower. The transverse momentum of the branchings was preserved in the case of multiple emission. The line shows the limits for the parton-shower emission for a single emission. $x_i = 2E_i/Q$ where E_i is the energy of parton i and Q is the centre-of-mass energy of the collision.

now a range of techniques which can achieve this including both the next-to-leading order normalization of the total cross section, or including the fixed-order results for multiple emissions. However, for our purposes it is sufficient to consider the simplest matrix-element correction approach where the *dead-zone* is filled using the leading-order matrix element for $e^+e^- \rightarrow q\bar{q}g$, as shown in Fig. 3, together with the reweighting of emission probability, Eqn. 6, to the exact leading-order result, for any emission which could have the highest transverse momentum in the parton shower.⁵

The choice of whether to preserve the transverse momentum or virtuality of the branching affects the phase-space region which is filled by the shower in the case of multiple emission. In this case we cluster the partons using the Durham jet algorithm [19], using the p-scheme as implemented in FastJet [20], keeping track of the partons emitted by the quark and antiquark and then take the hardest additional jet to be the gluon. The resulting Dalitz plots of $e^+e^- \rightarrow q\bar{q}$ show that while the choice to preserve the transverse momentum of the branching leads to a significant number of events in the *dead-zone*, Fig. 4, if the virtuality of the branching is preserved, Fig. 5, there is little emission outside the original angular-ordered region.

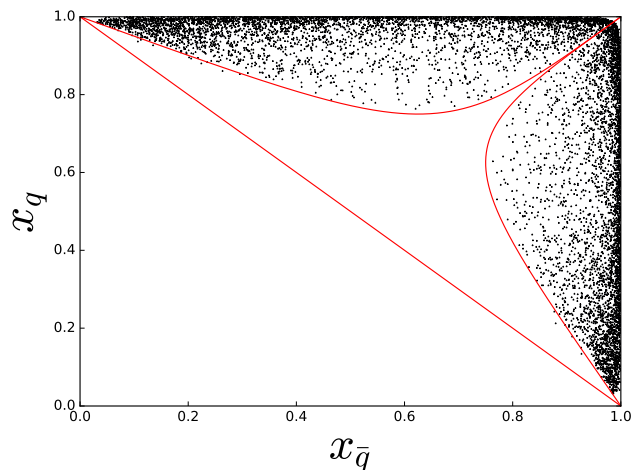


Fig. 5 Dalitz plot for $e^+e^- \rightarrow q\bar{q}$ showing the region of phase space filled after multiple emission from the quark and antiquark in the angular-ordered parton shower. The virtuality of the branchings was preserved in the case of multiple emission. The line shows the limits for the parton-shower emission for a single emission. $x_i = 2E_i/Q$ where E_i is the energy of parton i and Q is the centre-of-mass energy of the collision.

3 Hadronization and Colour Reconnection

All the Herwig family of event generator generators use the cluster hadronization model [21]. This model is based on the phenomena of colour pre-confinement, i.e. if we non-perturbatively split the gluons left at the end of the parton shower into quark-antiquark pairs and cluster quarks and antiquarks into colour-singlet clusters the mass spectrum of these clusters is peaked at masses close to the cut-off in the parton shower, falls rapidly as the cluster mass increases, and is universal, i.e. the mass distribution of these clusters is independent of the hard scattering process and its centre-of-mass energy. The cluster model assumes that these clusters are a superposition of heavy hadronic states and uses a simple phase-space model for their decay into two hadrons. The main parameters of the model are therefore:

- the non-perturbative gluon mass, which is not very sensitive and we do not tune;
- the parameters which control the probability of producing baryons and strange quarks during cluster decay;
- the parameter which controls the Gaussian smearing of the direction of the hadrons produced which contain a parton from the perturbative evolution about the direction of that parton, with separate values for light, charm and bottom quarks.

There are however a small fraction of large mass clusters for which the two hadron decay ansatz is not reasonable and these must first be fissioned into lighter clusters. While only a small fraction of clusters undergo fission due to the larger

⁵Due to the choice of ordering variable the hardest emission may not be the one that has the highest value of the ordering variable, i.e. the hardest emission may be not the first emission.

masses of these clusters they produce a significant fraction of the hadrons.

A cluster is split into two clusters if the mass, M , is such that

$$M^{\text{Cl}_{\text{pow}}} \geq \text{Cl}_{\text{max}}^{\text{Cl}_{\text{pow}}} + (m_1 + m_2)^{\text{Cl}_{\text{pow}}}, \quad (8)$$

where Cl_{max} and Cl_{pow} are parameters of the model, and $m_{1,2}$ are the masses of the constituent partons of the cluster.

For clusters that need to be split, a $q\bar{q}$ pair is selected to be popped from the vacuum. The mass distribution of the new clusters is given by

$$M_1 = m_1 + (M - m_1 - m_q) \mathcal{R}_1^{1/P_{\text{split}}}, \quad (9a)$$

$$M_2 = m_2 + (M - m_2 - m_q) \mathcal{R}_2^{1/P_{\text{split}}}, \quad (9b)$$

where m_q is the mass of the parton popped from the vacuum, $M_{1,2}$ are the masses of the clusters formed by the splitting and $\mathcal{R}_{1,2}$ are pseudo-random numbers uniformly distributed between 0 and 1. The distribution of the masses of the clusters is controlled by the parameter P_{split} .

In order to improve the description of charm and bottom hadron production these parameters for cluster fission all depend on the flavour of the partons in the cluster so that there are separate parameters for light, charm and bottom quarks.

In practice there is always a small fraction of clusters that are too light to decay into two hadrons. Before Herwig 7.1 these clusters were decayed to the lightest hadron, with the appropriate flavours. However in some cases, for example for clusters containing a charm or bottom quark-antiquark pair, or a bottom quark and a light antiquark, there can be a number of hadrons of the appropriate flavour below the threshold. In these cases the lightest meson with the appropriate flavours is the pseudoscalar 1S_0 state and the vector 3S_1 state is also below the threshold⁶ which leads to a lower production rate for the vector state with respect to the pseudoscalar state than expected. For the mesons composed of a bottom quark and a light quark the rate is significantly less than that expected from the counting of spin states, or indeed observed experimentally [22–25]. For charmonium and bottomonium states as this mechanism is the only way the vector states can be produced via hadronization it leads to a complete absence of direct J/ψ and Υ production. In Herwig 7.1 we therefore include the possibility that instead of just producing the lightest state all states below the threshold are produced with a probability proportional to $2S + 1$, where S is the spin of the particle.

In order to improve the behaviour at the threshold for charm and bottom clusters the option exists of allowing clusters above the threshold mass, $M_{\text{threshold}}$, for the production

of two hadrons to decay into a single hadron such that a single hadron can be formed for masses

$$M < M_{\text{limit}} = (1 + \text{SingleHadronLimit})M_{\text{threshold}}, \quad (10)$$

where **SingleHadronLimit** is a free parameter of the model. The probability of such a single-meson cluster decay is assumed to decrease linearly for $M_{\text{threshold}} < M < M_{\text{limit}}$ and there are separate parameters for charm and bottom clusters.

In order to explain the rising trend of $\langle p_t \rangle$ vs N_{ch} (average transverse momentum as a function of the number of charged particles in the event) observed already by UA1 [26] and describe Underlying Event [27–30] and the Minimum Bias data [31–34], the hadronization model is supplemented with a model of colour reconnections (CR) [35]. The default version of the model implemented in Herwig 7.0 is not very sophisticated. The colour reconnection model defines the distance between two partons based on their invariant mass, i.e. the distance is small when their invariant mass (cluster mass) is small. The aim of the CR model is to reduce the colour length $\lambda \equiv \sum_{i=1}^{N_{cl}} m_i^2$, where N_{cl} is the number of clusters in an event and m_i is the invariant mass of cluster i . The colour reconnection of the clusters leading to a reduction of λ is accepted with a given probability which is a parameter of the model. Although the default model is quite simple it should be stressed that its results resemble the more sophisticated statistical colour reconnection model [35] which implements the minimization of λ as Metropolis-like algorithm and requires a quick “cooling” of the random walk.

In this model the only possible reconnections which are not allowed are connecting the quark and antiquark produced in the non-perturbative splitting of the gluon. It is therefore possible that the colour lines of a gluon produced at any other stage of the shower can be reconnected leading to the production of a colour-singlet object. While this is physically possible we would expect that it occurs at a rate which is suppressed in the number of colours, N_C , as $\sim \frac{1}{N_C} = \frac{1}{9}$, not the much higher reconnection rate $\sim 2/3$ ⁷ which is necessary to describe the underlying event data. This can lead to the production of a colour-singlet gluon jet at a much higher rate than expected. This is particularly problematic in the theoretically clean, but experimentally inaccessible, colour-singlet gluon pair production processes often used to study gluon jets [9].

Consider, for example, the simple process of colour-singlet gluon pair production followed by the branching of all the gluons via $g \rightarrow gg$, shown in Fig. 6a. After the non-perturbative splitting of the gluons into quark-antiquark pairs, as shown in Fig. 6b, without colour reconnection the quarks and antiquarks will be formed into colour-singlet clusters as (q_1, \bar{q}_3) , (q_3, \bar{q}_4) , (q_4, \bar{q}_2) and (q_2, \bar{q}_1) . Given the configuration it is likely that the clusters containing partons from the

⁶For charmonium and bottomonium states there are a number of other states below the threshold.

⁷The value from the tune of Herwig 7.1 with a new soft and diffractive model [36].



Fig. 6 Example of colour-singlet gluon pair production followed by the branching of all the colours via $g \rightarrow gg$. The Feynman diagram is shown in (a) whereas the colour flows, including the non-perturbative splitting of the gluons into quark-antiquark pairs is shown in (b).

parton shower of each of the original gluons, i.e. (q_1, \bar{q}_3) and (q_4, \bar{q}_2) , will have large masses and the rearrangement to give the clusters (q_1, \bar{q}_2) and (q_4, \bar{q}_3) will be kinematically favoured, although it means the original gluons will effectively become colour singlets rather than octets.

In Herwig 7.1 we have therefore included the possibility to forbid the colour reconnection model making any reconnection which would lead to a gluon produced in any stage of the parton-shower evolution becoming a colour-singlet after hadronization. We will investigate the effect of this change on the simulation of quark and gluon jets.

4 Tuning

The Rivet [37] program was used to analyse the simulated events and compare the results with the experimental measurements. The Professor program [38] was then used to interpolate the shower response and tune the parameters by minimising the chi-squared.⁸

In general we use a heuristic chi-squared function

$$\chi^2(p) = \sum_{\mathcal{O}} w_{\mathcal{O}} \sum_{b \in \mathcal{O}} \frac{(f_b(p) - \mathcal{R}_b)^2}{\Delta_b^2} \quad (11)$$

where p is the set of parameters being tuned, \mathcal{O} are the observables used each with weight $w_{\mathcal{O}}$, b are the different bins in each observable distribution with associated experimental measurement \mathcal{R}_b , error Δ_b and Monte Carlo prediction $f_b(p)$. Weighting of those observables for which a good description of the experimental result is important is used in most cases. The parameterisation of the event generator response, $f(p)$, is used to minimize χ^2 and find the optimum parameter values. We take $w_{\mathcal{O}} = 1$ in most cases except for the particle multiplicities where we use $w_{\mathcal{O}} = 10$ and total charged particle multiplicities where we use $w_{\mathcal{O}} = 50$. This ensures that particle multiplicities influence the result of the fit and are required due to the much higher quantity of event

⁸While tuning the parameters sensitive to bottom quarks it proved impossible to get a reliable interpolation of the generator response with Professor and therefore a random scan of the bottom parameters was performed and the values adjusted by hand about the minimum to minimise the χ^2 .

shape and spectrum data used in the tuning. Given the aim of this paper is to improve the description of gluon jets this data was also included with $w_{\mathcal{O}} = 10$ in order to avoid the fit being dominated by the large quantity of data sensitive to quark jets. In addition as we do not expect a Monte Carlo event generator to give a perfect description of all the data and in order to avoid the fit being dominated by a few observables with very small experimental errors we use

$$\Delta_b^{\text{eff}} = \max(0.05 \times \mathcal{R}_b, \Delta_b), \quad (12)$$

rather than the true experimental error, Δ_b , in the fit.

The standard procedure which was adopted to tune the shower and hadronization parameters of the Herwig++ and Herwig 7 event generators to data is

- first the shower and those hadronization parameters which are primarily sensitive to light quark-initiated processes are tuned to LEP1 and SLD measurements of event shapes, the average charged multiplicity and charged multiplicity distribution, and identified particle spectra and rates which only involve light quark mesons and baryons;
- the hadronization parameters for bottom quarks are tuned to the bottom quark fragmentation function measured by LEP1 and SLD together with LEP1 and SLD measurements of event shapes and identified particle spectra from bottom events;
- the hadronization parameters involving charm quarks are then tuned to identified particle spectra, from both the B-factories and LEP1, and LEP1 and SLD measurements of event shapes and identified particle spectra from charm events;
- the light quark parameters are then retuned using the new values of the bottom and charm parameters together with different weights for the charged multiplicity distributions in e^+e^- collisions at energies between 12 GeV and 209 GeV due to the difficulty in fitting the charged multiplicity.

Only e^+e^- annihilation data from the continuum region near the $Y(4s)$ meson, for charm meson spectra, and at the Z -pole from LEP1 and SLD were used in the tune.

In this paper we have extended this approach in order to better constrain the energy evolution to include data from a wider range of centre-of-mass energies both below the Z-pole, from the JADE and TASSO experiments, and above the Z-pole, from LEP2.

In order to tune the shower and light quark hadronization parameters we used data on jet rates and event shapes for centre-of-mass energies between 14 and 44 GeV [39–41], at LEP1 and SLD [41–45] and LEP2 [41, 44, 45], particle multiplicities [42, 43] and spectra [42, 43, 46–56] at LEP 1, identified particle spectra below the $Y(4S)$ from Babar [57], the charged particle multiplicity [58, 59] and particle spectra [58, 60, 61] in light quark events at LEP1 and SLD, the charged particle multiplicity in light quark events at LEP2 [62, 63], the charged particle multiplicity distribution at LEP 1 [64], and hadron multiplicities at the Z-pole [65]. We also implemented in Rivet and made use of the data on the properties of gluon jets [11, 12] for the first time.

The hadronization parameters for charm quarks were tuned using the charged multiplicity in charm events at SLD [59] and LEP2 [62, 63], the light hadron spectra in charm events at LEP1 and SLD [58, 60, 61], the multiplicities of charm hadrons at the Z-pole [42, 65], and charm hadron spectra below the $Y(4S)$ [66, 67] and at LEP1 [68].

The hadronization parameters for bottom quarks were tuned using the charged multiplicity in bottom events at SLD [59] and LEP2 [62, 63], the light hadron spectra in bottom events at LEP1 and SLD [58, 60, 61], the multiplicities of charm and bottom hadrons at the Z-pole [42, 65], charm hadron spectra at LEP1 [68] and the bottom fragmentation function measured at LEP1 and SLD [69–71].

In order to tune the evolution of the total charged particle multiplicity in e^+e^- collisions as a function of energy the results of Refs. [42, 45, 59, 62, 63, 72–78] spanning energies from 12 to 209 GeV were used.

In order to study the various effects we have discussed we have produced tunes for the shower and hadronization parameters in the case that either the transverse momentum or virtuality in the shower is preserved. In each case we first tuned the shower and light quark parameters without the data on charged particle multiplicities as centre-of-mass energies below the mass of the Z^0 boson. In the final stage of the process where we retune these parameters three tunes were produced for each choice of cut-off and preserved quantity, one (labelled A) without the low-energy charged multiplicity data, one (labelled B) where all the charged multiplicity data was included with in the tune with weight $w_\phi = 100$ and a final tune (labelled C) where this data had weight $w_\phi = 1000$.

Unfortunately due to the CPU time required it is impossible to include the ATLAS data [10] directly in the tune, therefore we compare the results of the different tunes to this data.

5 Results

We have produced 12 tunes for different choices of the cut-off variable in the shower, the choice of which quantity to preserve in the parton shower, and different weightings of the charged particle multiplicities. The parameters obtained in the fits are given in Table. 1 while the χ^2 values are given in Table. 2.

The effects of changing the colour reconnection model can be seen in Fig. 7. In the results of Herwig++ 2.7.1 or Herwig 7.0 there is an unphysical tendency of the gluon jets to contain an even number of charged particles due to the production of colour-singlet gluons by the reconnection model, this feature is not present in any of the new tunes which provide a much better description of the distribution of charged particles in the gluon jets, see also the Appendix.

The choice of which tune and choice of cut-off variable and preserved quantity has to be a balance between how well we wish to describe the various different data sets, as unfortunately no choice provides a good description of all the data sets.

If we first consider the choice of cut-off it is clear that using a virtual mass provides a larger χ'^2 for all sets of observables used in the tuning apart from those sensitive to bottom quarks. In addition it displays an unphysical energy dependence in the difference in charged particle multiplicities between bottom (or charm) quark and light quark events, as shown in Fig. 8 where the results which use a cut-off on the virtual mass, Herwig++ 2.7.1 and the new tune q^2 - q^2 -B, show a strong dependence on the centre-of-mass energy while those which use a p_\perp cut-off, Herwig 7.0 and the new tune p_\perp - q^2 -B, are relatively independent of energy. We therefore prefer a cut-off on the minimum transverse momentum of the branching.

In order to obtain a reasonable evolution of the number of charged particles with centre-of-mass energy in e^+e^- collisions, see Fig. 9, without ruining the description of particle spectra and event shape observables we choose to use the B tune as our default.

The choice of whether to preserve the p_\perp or q^2 of the branching is more complicated. While the data on light quark jets, in particular event shapes measured at LEP (for example the thrust Fig. 10), favour preserving q^2 the data on the charged particle multiplicity in gluon jets at LEP Fig. 11, and in jets at the LHC Figs. 12,13 favours preserving the p_\perp of the branching.

Our preferred choice, in particular in the presence of higher-order matching, is to preserve the q^2 of the branching in order to ensure that the parton shower does not overpopulate the dead-zone. This also ensures a more reasonable value of strong coupling, $\alpha_S^{\text{CMW}}(M_Z) = 0.126$ which gives $\alpha_S^{\text{MS}}(M_Z) = 0.118$. However given the better description of gluon jets it is reasonable to also consider the alternative of

| Cut-Off | p_{\perp} | | | | | | Virtual Mass | | | | | |
|---|-------------|--------|--------|--------|--------|--------|--------------|--------|--------|--------|--------|--------|
| Preserved Tune | p_{\perp} | | | q^2 | | | p_{\perp} | | | q^2 | | |
| | A | B | C | A | B | C | A | B | C | A | B | C |
| Bottom quark hadronization parameters | | | | | | | | | | | | |
| CIMaxBottom | 4.655 | | | 3.911 | | | 4.0612 | | | 4.163 | | |
| CIPowBottom | 0.622 | | | 0.638 | | | 0.9475 | | | 0.590 | | |
| PSplitBottom | 0.499 | | | 0.531 | | | 1.9568 | | | 1.881 | | |
| CISmrBottom | 0.082 | | | 0.020 | | | 0.04 | | | 0.040 | | |
| SingleHadronLimitBottom | 0.000 | | | 0.000 | | | 0.0204 | | | 0.000 | | |
| Charm quark hadronization parameters | | | | | | | | | | | | |
| SingleHadronLimitCharm | 0.000 | | | 0.000 | | | 0.078 | | | 0.012 | | |
| CIMaxCharm | 3.551 | | | 3.638 | | | 3.805 | | | 3.885 | | |
| CIPowCharm | 1.923 | | | 2.332 | | | 2.242 | | | 2.452 | | |
| PSplitCharm | 1.260 | | | 1.234 | | | 1.895 | | | 1.767 | | |
| CISmrCharm | 0.000 | | | 0.000 | | | 0.000 | | | 0.000 | | |
| Light quark hadronization and shower parameters | | | | | | | | | | | | |
| AlphaMZ ($\alpha_S^{CMW}(M_Z)$) | 0.1094 | 0.1087 | 0.1126 | 0.1260 | 0.1262 | 0.1265 | 0.1221 | 0.1218 | 0.1184 | 0.1314 | 0.1317 | 0.1254 |
| pTmin | 1.037 | 0.933 | 0.809 | 1.301 | 1.223 | 0.992 | N/A | | | N/A | | |
| aParameter | N/A | | | N/A | | | 0.367 | | | 0.234 | | |
| cutoffKinScale | N/A | | | N/A | | | 2.939 | 2.910 | 2.294 | 3.277 | 3.279 | 1.938 |
| CIMaxLight | 3.504 | 3.639 | 4.349 | 3.058 | 3.003 | 3.197 | 3.328 | 3.377 | 3.846 | 3.414 | 3.427 | 3.477 |
| CIPowLight | 2.576 | 2.575 | 1.226 | 1.513 | 1.424 | 2.786 | 1.286 | 1.318 | 2.063 | 2.766 | 2.792 | 2.35 |
| PSplitLight | 1.003 | 1.016 | 0.855 | 0.885 | 0.848 | 0.648 | 1.198 | 1.185 | 1.277 | 1.346 | 1.333 | 2.015 |
| PwtSquark | 0.552 | 0.597 | 1.167 | 0.602 | 0.666 | 1.024 | 0.721 | 0.741 | 0.782 | 0.626 | 0.646 | 1.15 |
| PwtDiquark | 0.369 | 0.344 | 0.181 | 0.416 | 0.439 | 0.512 | 0.277 | 0.273 | 0.246 | 0.321 | 0.328 | 0.366 |

Table 1 The Monte Carlo parameters obtained for different choices of the cut-off option, the preserved quantity in the shower and weight of the charged particle multiplicity data.

| Cut-Off | p_{\perp} | | | | | | Virtual Mass | | | | | | Number of degrees of freedom (sum including weights) |
|----------------------|-------------|------|------|-------|------|------|--------------|------|------|-------|------|------|--|
| Preserved Tune | p_{\perp} | | | q^2 | | | p_{\perp} | | | q^2 | | | |
| | A | B | C | A | B | C | A | B | C | A | B | C | |
| Tuning Observables | | | | | | | | | | | | | |
| Light quarks | 4.4 | 4.3 | 6.7 | 3.0 | 2.9 | 4.2 | 7.8 | 7.6 | 6.9 | 4.6 | 4.3 | 3.6 | 10122(14099) |
| Charm quarks | 3.2 | 2.8 | 5.8 | 3.6 | 3.5 | 3.9 | 4.5 | 4.6 | 6.4 | 3.9 | 3.9 | 7.4 | 549(891) |
| Bottom quarks | 4.0 | 3.4 | 3.6 | 5.4 | 4.9 | 3.4 | 3.4 | 3.3 | 3.4 | 4.1 | 4.1 | 4.9 | 346(1309) |
| Gluons | 1.1 | 1.1 | 1.5 | 1.1 | 1.1 | 1.4 | 1.2 | 1.2 | 1.2 | 1.3 | 1.2 | 1.5 | 188(1880) |
| N_{charged} | | | | | | | | | | | | | |
| Gluon | 14.2 | 18.6 | 22.6 | 26.9 | 37.1 | 60.0 | 3.4 | 3.7 | 8.1 | 10.0 | 11.0 | 22.8 | 26 |
| All quarks | 4.6 | 2.7 | 2.7 | 3.4 | 2.5 | 5.2 | 11.6 | 10.7 | 3.7 | 7.2 | 6.5 | 1.6 | 48 |
| Light quarks | 2.2 | 1.7 | 2.8 | 1.7 | 1.8 | 4.4 | 4.8 | 4.4 | 2.1 | 3.9 | 3.5 | 1.8 | 27 |
| Charm quarks | 2.8 | 2.0 | 1.1 | 2.2 | 1.6 | 1.0 | 2.8 | 2.6 | 1.2 | 2.2 | 2.2 | 0.9 | 17 |
| Bottom quarks | 20.4 | 18.1 | 15.8 | 24.1 | 21.3 | 15.7 | 33.4 | 33.1 | 34.7 | 22.0 | 21.5 | 46.2 | 27 |
| ATLAS Jets | 3.2 | 0.9 | 4.3 | 13.3 | 10.1 | 7.8 | 21.8 | 19.0 | 6.4 | 33.3 | 31.3 | 38.0 | 22 |

Table 2 The values of χ^2 per degree of freedom obtained in the fit for different choices of the cut-off option, the preserved quantity in the shower and weight of the charged particle multiplicity data. The values are χ^2 as described in the text for the tuning observables, normalised to the sum of the weights for the different bins, and the true χ^2 using the experimental error for the charged particle multiplicities. The number of degrees of freedom for each set of observables is given together with the sum including weights in brackets, where this is different.

preserving the p_{\perp} , see for example Fig. 16 from the Appendix.

6 Conclusions

We have performed a tuning the the Herwig 7 event generator using data on gluon jets from LEP for the first time. To-

gether with changes to the non-perturbative modelling this gives a significantly better description of gluon jets, in particular their charge particle multiplicity. It is however impossible to get a good description of the LEP particle spectra and the charged particle multiplicities, particularly in gluon jets, at the same time. We therefore choose the tune p_{\perp} - q^2 -B as the default for Herwig 7.1. However for jets at the LHC the tune p_{\perp} - p_{\perp} -B gives a better description of jet properties.

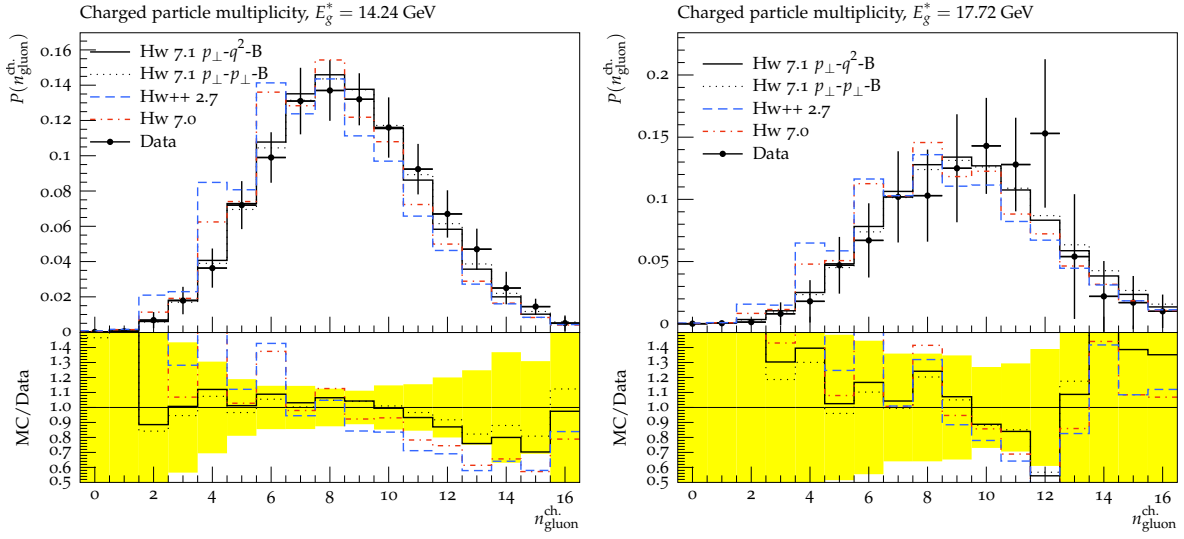


Fig. 7 Multiplicity distribution of charged particles in gluons jets for two different gluon energies compared to data from OPAL [11].

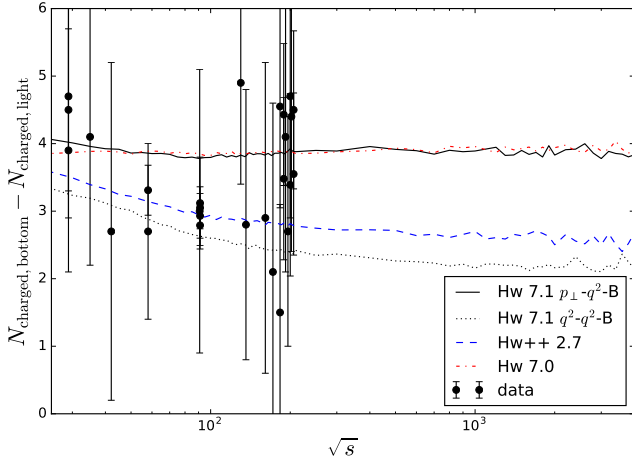


Fig. 8 Difference between the charged multiplicity in bottom and light quark events in e^+e^- collisions as a function of centre-of-mass energy. The data is from [59, 61–63, 73, 79–88] as compiled in [89]

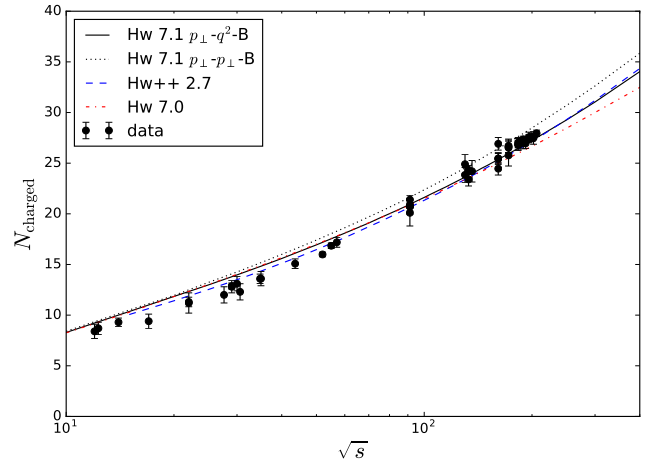


Fig. 9 The evolution of the number of charged particles in $e^+e^- \rightarrow$ hadrons as a function of the centre-of-mass energy.

While the tunes presented in this paper are an improvement on their predecessors there is a tension between the data on charged particle multiplicities, for both quark and gluon initiated jets, and the data on event shapes and particle spectra from LEP. The cluster hadronization model also continues to have problems describing final states in events with bottom quarks. Any further improvement in the description of this data will require improvements to the non-perturbative modelling.

Acknowledgements This work was supported in part by the European Union as part of the FP7 and H2020 Marie Skłodowska-Curie Initial Training Networks MCnetITN and MCnetITN3 (PITN-GA-2012-315877 and 722104). Daniel Reichelt thanks CERN for the award of a summer studentship during which this work was initiated and acknowl-

edges support from the German Research Foundation (DFG) under grant No. SI 2009/1-1. Andrzej Siodmok acknowledges support from the National Science Centre, Poland Grant No. 2016/23/D/ST2/02605. We thank our collaborators on Herwig for many useful discussions. The tuning of Herwig to experimental data would not have been possible without the use of GRIDPP computer resources.

Appendix A: Generalized angularities and quark and gluon jet discrimination power

In this appendix we investigate how the improvements of the simulation of quark and gluon proposed in the manuscript affect the quark and gluon jet discrimination power recently

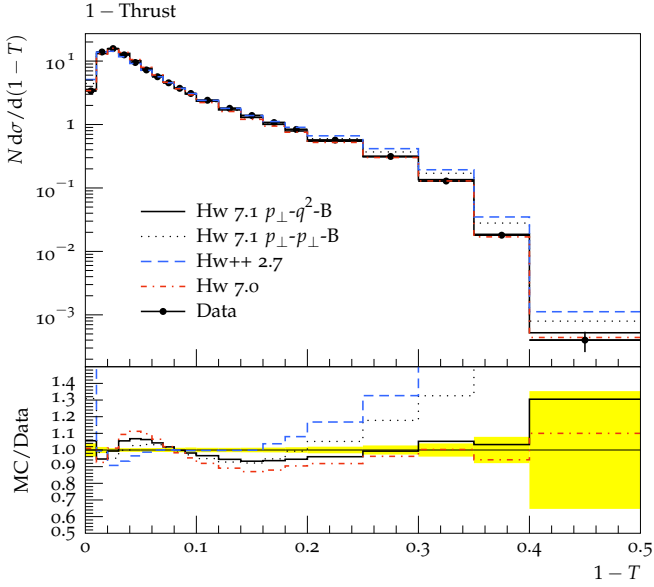


Fig. 10 The thrust at the Z-pole compared to data from the DELPHI [42] experiment.

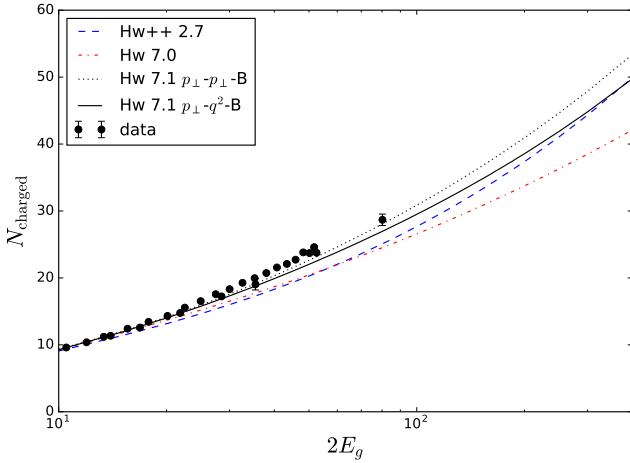


Fig. 11 The evolution of the number of charged particles in gluon jets as a function of twice the energy of the gluon jet.

studied in [9]⁹. For this purpose, we present results for five generalized angularities λ_β^κ [90]:

$$\begin{array}{cccccc}
 (\kappa, \beta) & (0,0) & (2,0) & (1,0.5) & (1,1) & (1,2) \\
 \lambda_\beta^\kappa & \text{multiplicity} & p_T^D & \text{LHA} & \text{width} & \text{mass}
 \end{array}$$

where $\lambda_\beta^\kappa = \sum_{i \in \text{jet}} z_i^\kappa \theta_i^\beta$, i runs over the jet constituents, $z_i \in [0, 1]$ is a momentum fraction, and $\theta_i \in [0, 1]$ is an angle to the jet axis. To quantify discrimination performance, we use

⁹The results and the analysis code used for this study is available as a RIVET routine [37], which can be downloaded from <https://github.com/gsoyez/lh2015-qg>.

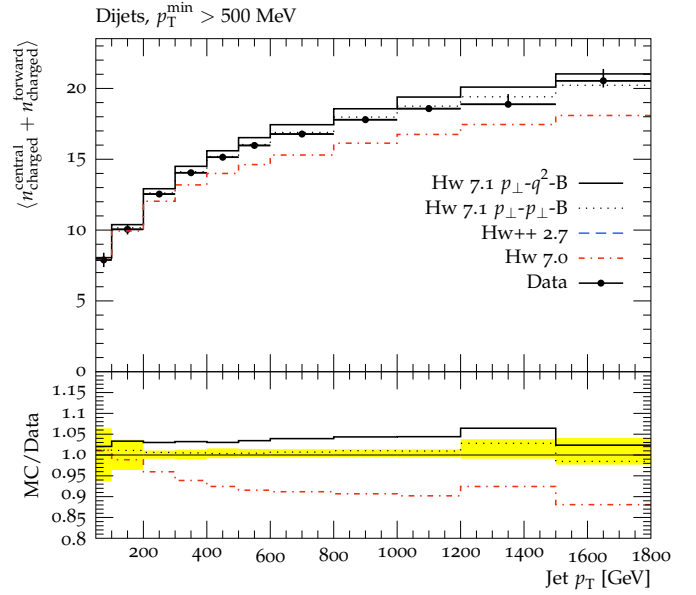


Fig. 12 The average number of charged particles in jets as a function of the jet transverse momentum compared to data from the ATLAS experiment [10].

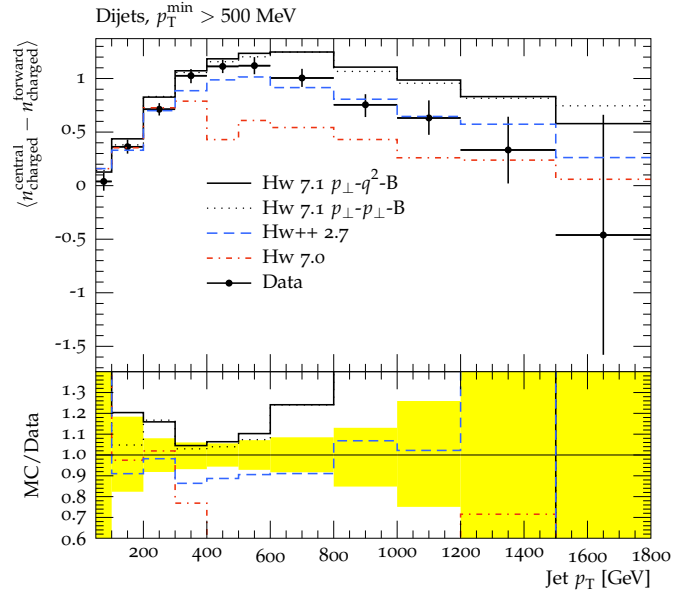


Fig. 13 The difference between the average number of particles in central and forward jets compared to data from the ATLAS experiment [10].

classifier separation:

$$\Delta = \frac{1}{2} \int d\lambda \frac{(p_q(\lambda) - p_g(\lambda))^2}{p_q(\lambda) + p_g(\lambda)},$$

where p_q (p_g) is the probability distribution for λ in a generated quark jet (gluon jet) sample. $\Delta = 0$ corresponds to no discrimination power and $\Delta = 1$ corresponds to perfect discrimination power.

We start with an idealized case of e^+e^- collisions (see Section 5 of [9] for details). In Fig. 14 we show the discrimination power as a function of an angularity predicted by PYTHIA 8.215 [2], HERWIG++ 2.7.1 [16], SHERPA 2.2.1 [3], the NNL analytical calculation from [9] and the both p_\perp - q^2 -B and p_\perp - p_\perp -B tunes of Herwig 7.1. Firstly, we see that the both Herwig 7.1 tunes give significantly different results compared to HERWIG++ 2.7.1. In order to understand the source of the difference, in Fig 15 we investigate, for p_\perp - q^2 -B tune, the following settings variations:

- HERWIG: NO $g \rightarrow q\bar{q}$. Turning off $g \rightarrow q\bar{q}$ splittings in the parton shower.
- HERWIG: NO CR. The variation turns off color reconnections.

We can see that the results are not very sensitive to the change of the settings. This was not the case for HERWIG++ 2.7.1 where the colour reconnection had a huge effect on the discrimination power, see [9]. Therefore, we can conclude that the difference is due to the improvements of the CR model described in Section 3, which as expected reduce effects of CR in the case of e^+e^- collisions. Secondly, the results of the both Herwig 7.1 tunes are quite similar and closer to the other predictions giving more constrained prediction on the quark/gluon jet discrimination power in e^+e^- collisions. In fact just before finishing this paper the new tune was used in [91] confirming that indeed that improvements introduced in the manuscript reduced the tension between Pythia and Herwig and bring Herwig results closer to NNLL' results from [91].

Next, in Fig. 16 we show the results for Δ in the case of quark/gluon tagging at the LHC (see Section 6 of [9] for details). Here we can see that the differences between HERWIG++ 2.7.1 and the both Herwig 7.1 tunes are more modest when compared to the previous case of e^+e^- collisions. However, as expected the largest differences between generators appear for IRC-unsafe observables like multiplicity (0,0) and p_T^D (2,0), where nonperturbative hadronization plays an important role. It is also worth to notice that the p_\perp - p_\perp -B tune which is preferred by the data on the charged particle multiplicity in gluon jets at LEP Fig. 11, and in jets at the LHC Figs. 12,13 gives slightly better discrimination power reducing the gap between predictions of Pythia and the other generators. Finally, it would be interesting to estimate the parton-shower uncertainties [92–95] in the context of the quark and gluon jet discrimination observables to see whether the remaining discrepancy in the predictions is covered by the uncertainty band.

References

1. J. Bellm, et al., Eur. Phys. J. **C76**(4), 196 (2016). DOI 10.1140/epjc/s10052-016-4018-8

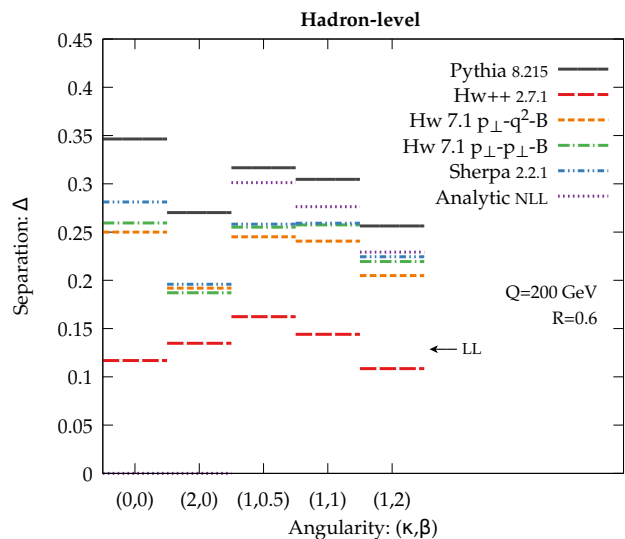


Fig. 14 Classifier separation Δ for the five angularities, determined from the various generators at hadron level for an idealized case of e^+e^- collisions. The first two columns correspond to IRC-unsafe distributions (multiplicity and p_T^D), while the last three columns are the IRC-safe angularities.

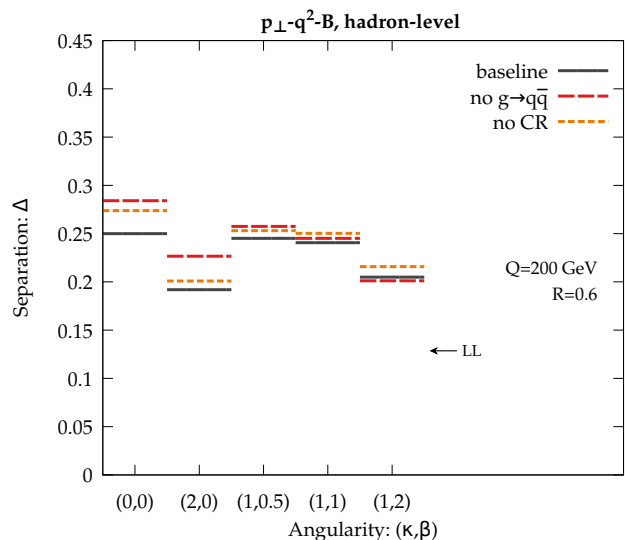


Fig. 15 Settings variations for Herwig 7.1 p_\perp - q^2 -B tune. Hadron-level results for the classifier separation Δ derived from the five benchmark angularities.

2. T. Sjöstrand, S. Ask, J.R. Christiansen, R. Corke, N. Desai, P. Ilten, S. Mrenna, S. Prestel, C.O. Rasmussen, P.Z. Skands, Comput. Phys. Commun. **191**, 159 (2015). DOI 10.1016/j.cpc.2015.01.024
3. T. Gleisberg, S. Hoeche, F. Krauss, M. Schönherr, S. Schumann, F. Siegert, J. Winter, JHEP **02**, 007 (2009). DOI 10.1088/1126-6708/2009/02/007
4. A. Buckley, et al., Phys. Rept. **504**, 145 (2011). DOI 10.1016/j.physrep.2011.03.005

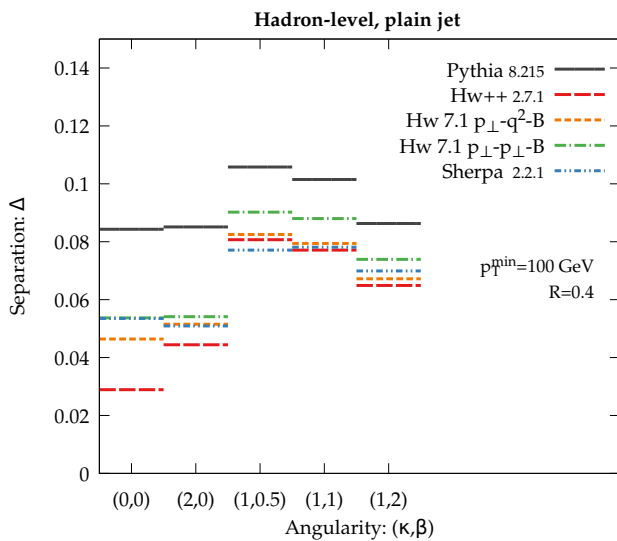


Fig. 16 Classifier separation Δ for the five angularities, determined from the various generators at hadron level in the case of quark/gluon tagging at the LHC (see Section 6 of [9] for details). The first two columns correspond to IRC-unsafe distributions (multiplicity and p_T^D), while the last three columns are the IRC-safe angularities.

5. G. Aad, et al., Eur. Phys. J. **C74**(8), 3023 (2014). DOI 10.1140/epjc/s10052-014-3023-z
6. V. Khachatryan, et al., JHEP **05**, 064 (2011). DOI 10.1007/JHEP05(2011)064
7. V. Khachatryan, et al., JHEP **09**, 091 (2010). DOI 10.1007/JHEP09(2010)091
8. G. Aad, et al., Phys. Rev. Lett. **116**(17), 172301 (2016). DOI 10.1103/PhysRevLett.116.172301
9. P. Gras, S. Hoeche, D. Kar, A. Larkoski, L. Lönnblad, S. Plätzer, A. Siódmok, P. Skands, G. Soyez, J. Thaler, JHEP **07**, 091 (2017). DOI 10.1007/JHEP07(2017)091
10. G. Aad, et al., Eur. Phys. J. **C76**(6), 322 (2016). DOI 10.1140/epjc/s10052-016-4126-5
11. G. Abbiendi, et al., Phys. Rev. **D69**, 032002 (2004). DOI 10.1103/PhysRevD.69.032002
12. G. Abbiendi, et al., Eur. Phys. J. **C37**(1), 25 (2004). DOI 10.1140/epjc/s2004-01964-4
13. S. Gieseke, P. Stephens, B. Webber, JHEP **12**, 045 (2003). DOI 10.1088/1126-6708/2003/12/045
14. G. Corcella, et al., JHEP **01**, 010 (2001)
15. S. Gieseke, A. Ribon, M.H. Seymour, P. Stephens, B. Webber, JHEP **02**, 005 (2004)
16. M. Bähr, et al., Eur. Phys. J. **C58**, 639 (2008). DOI 10.1140/epjc/s10052-008-0798-9
17. S. Catani, B.R. Webber, G. Marchesini, Nucl. Phys. **B349**, 635 (1991)
18. S. Gieseke, M.H. Seymour, A. Siódmok, JHEP **06**, 001 (2008). DOI 10.1088/1126-6708/2008/06/001
19. S. Catani, Yu.L. Dokshitzer, M. Olsson, G. Turnock, B.R. Webber, Phys. Lett. **B269**, 432 (1991). DOI 10.1016/0370-2693(91)90196-W
20. M. Cacciari, G.P. Salam, G. Soyez, Eur. Phys. J. **C72**, 1896 (2012). DOI 10.1140/epjc/s10052-012-1896-2
21. B.R. Webber, Nucl. Phys. **B238**, 492 (1984). DOI 10.1016/0550-3213(84)90333-X
22. M. Acciarri, et al., Phys. Lett. **B345**, 589 (1995). DOI 10.1016/0370-2693(95)01611-S
23. P. Abreu, et al., Z. Phys. **C68**, 353 (1995)
24. D. Buskulic, et al., Z. Phys. **C69**, 393 (1996). DOI 10.1007/BF02907419
25. K. Ackerstaff, et al., Z. Phys. **C74**, 413 (1997). DOI 10.1007/s002880050404
26. C. Albajar, et al., Nucl. Phys. **B335**, 261 (1990). DOI 10.1016/0550-3213(90)90493-W
27. T. Affolder, et al., Phys. Rev. **D65**, 092002 (2002). DOI 10.1103/PhysRevD.65.092002
28. G. Aad, et al., Phys. Rev. **D83**, 112001 (2011). DOI 10.1103/PhysRevD.83.112001
29. S. Chatrchyan, et al., JHEP **09**, 109 (2011). DOI 10.1007/JHEP09(2011)109
30. M.H. Seymour, A. Siódmok, JHEP **10**, 113 (2013). DOI 10.1007/JHEP10(2013)113
31. G. Aad, et al., New J. Phys. **13**, 053033 (2011). DOI 10.1088/1367-2630/13/5/053033
32. G. Aad, et al., Phys. Lett. **B758**, 67 (2016). DOI 10.1016/j.physletb.2016.04.050
33. G. Aad, et al., Eur. Phys. J. **C76**(7), 403 (2016). DOI 10.1140/epjc/s10052-016-4203-9
34. M. Aaboud, et al., Eur. Phys. J. **C76**(9), 502 (2016). DOI 10.1140/epjc/s10052-016-4335-y
35. S. Gieseke, C. Rohr, A. Siódmok, Eur. Phys. J. **C72**, 2225 (2012). DOI 10.1140/epjc/s10052-012-2225-5
36. S. Gieseke, F. Loshaj, P. Kirchgaerber, Eur. Phys. J. **C77**(3), 156 (2017). DOI 10.1140/epjc/s10052-017-4727-7
37. A. Buckley, J. Butterworth, L. Lönnblad, D. Grellscheid, H. Hoeth, J. Monk, H. Schulz, F. Siegert, Comput. Phys. Commun. **184**, 2803 (2013). DOI 10.1016/j.cpc.2013.05.021
38. A. Buckley, H. Hoeth, H. Lacker, H. Schulz, J.E. von Seggern, Eur. Phys. J. **C65**, 331 (2010). DOI 10.1140/epjc/s10052-009-1196-7
39. W. Braunschweig, et al., Z. Phys. **C47**, 187 (1990). DOI 10.1007/BF01552339
40. P.A. Movilla Fernandez, O. Biebel, S. Bethke, S. Kluth, P. Pfeifenschneider, Eur. Phys. J. **C1**, 461 (1998). DOI 10.1007/s100520050096
41. P. Pfeifenschneider, et al., Eur. Phys. J. **C17**, 19 (2000). DOI 10.1007/s100520000432
42. P. Abreu, et al., Z. Phys. **C73**, 11 (1996). DOI 10.1007/s002880050295
43. R. Barate, et al., Phys. Rept. **294**, 1 (1998). DOI 10.1016/S0370-1573(97)00045-8

44. G. Abbiendi, et al., Eur. Phys. J. **C40**, 287 (2005). DOI 10.1140/epjc/s2005-02120-6
45. A. Heister, et al., Eur. Phys. J. **C35**, 457 (2004). DOI 10.1140/epjc/s2004-01891-4
46. R. Akers, et al., Z. Phys. **C63**, 181 (1994). DOI 10.1007/BF01411010
47. G. Alexander, et al., Phys. Lett. **B358**, 162 (1995). DOI 10.1016/0370-2693(95)00935-E
48. G. Alexander, et al., Z. Phys. **C70**, 197 (1996). DOI 10.1007/s002880050096
49. P. Abreu, et al., Z. Phys. **C67**, 543 (1995). DOI 10.1007/BF01553980
50. G. Alexander, et al., Z. Phys. **C73**, 569 (1997). DOI 10.1007/s002880050349
51. K. Ackerstaff, et al., Phys. Lett. **B412**, 210 (1997). DOI 10.1016/S0370-2693(97)01077-0
52. P. Abreu, et al., Phys. Lett. **B449**, 364 (1999). DOI 10.1016/S0370-2693(99)00105-7
53. K. Ackerstaff, et al., Eur. Phys. J. **C5**, 411 (1998). DOI 10.1007/s100520050286
54. K. Ackerstaff, et al., Eur. Phys. J. **C4**, 19 (1998). DOI 10.1007/s100520050183
55. G. Abbiendi, et al., Eur. Phys. J. **C17**, 373 (2000). DOI 10.1007/s100520000505
56. A. Heister, et al., Phys. Lett. **B528**, 19 (2002). DOI 10.1016/S0370-2693(02)01220-0
57. J.P. Lees, et al., Phys. Rev. **D88**, 032011 (2013). DOI 10.1103/PhysRevD.88.032011
58. K. Ackerstaff, et al., Eur. Phys. J. **C7**, 369 (1999). DOI 10.1007/s100529901067
59. K. Abe, et al., Phys. Lett. **B386**, 475 (1996). DOI 10.1016/0370-2693(96)01025-8
60. K. Abe, et al., Phys. Rev. **D59**, 052001 (1999). DOI 10.1103/PhysRevD.59.052001
61. K. Abe, et al., Phys. Rev. **D69**, 072003 (2004). DOI 10.1103/PhysRevD.69.072003
62. P. Abreu, et al., Phys. Lett. **B479**, 118 (2000). DOI 10.1016/S0370-2693(00)01086-8, 10.1016/S0370-2693(00)00312-9. [Erratum: Phys. Lett. **B492**, 398 (2000)]
63. G. Abbiendi, et al., Phys. Lett. **B550**, 33 (2002). DOI 10.1016/S0370-2693(02)02935-0
64. D. Decamp, et al., Phys. Lett. **B273**, 181 (1991). DOI 10.1016/0370-2693(91)90575-B
65. C. Amsler, et al., Phys. Lett. **B667**, 1 (2008). DOI 10.1016/j.physletb.2008.07.018
66. R. Seuster, et al., Phys. Rev. **D73**, 032002 (2006). DOI 10.1103/PhysRevD.73.032002
67. B. Aubert, et al., Phys. Rev. **D75**, 012003 (2007). DOI 10.1103/PhysRevD.75.012003
68. R. Barate, et al., Eur. Phys. J. **C16**, 597 (2000). DOI 10.1007/s100520000421
69. K. Abe, et al., Phys. Rev. **D65**, 092006 (2002). DOI 10.1103/PhysRevD.66.079905, 10.1103/PhysRevD.65.092006. [Erratum: Phys. Rev. **D66**, 079905 (2002)]
70. A. Heister, et al., Phys. Lett. **B512**, 30 (2001). DOI 10.1016/S0370-2693(01)00690-6
71. J. Abdallah, et al., Eur. Phys. J. **C71**, 1557 (2011). DOI 10.1140/epjc/s10052-011-1557-x
72. M. Derrick, et al., Phys. Rev. **D34**, 3304 (1986). DOI 10.1103/PhysRevD.34.3304
73. H. Aihara, et al., Phys. Lett. **B184**, 299 (1987). DOI 10.1016/0370-2693(87)90586-7
74. C. Berger, et al., Phys. Lett. **B95**, 313 (1980). DOI 10.1016/0370-2693(80)90494-3
75. W. Bartel, et al., Z. Phys. **C20**, 187 (1983)
76. W. Braunschweig, et al., Z. Phys. **C45**, 193 (1989). DOI 10.1007/BF01674450
77. H.W. Zheng, et al., Phys. Rev. **D42**, 737 (1990). DOI 10.1103/PhysRevD.42.737
78. P.D. Acton, et al., Z. Phys. **C53**, 539 (1992). DOI 10.1007/BF01559731
79. P.C. Rowson, et al., Phys. Rev. Lett. **54**, 2580 (1985). DOI 10.1103/PhysRevLett.54.2580
80. M. Sakuda, et al., Phys. Lett. **B152**, 399 (1985). DOI 10.1016/0370-2693(85)90518-0
81. W. Braunschweig, et al., Z. Phys. **C42**, 17 (1989). DOI 10.1007/BF01565125
82. M. Althoff, et al., Phys. Lett. **B135**, 243 (1984). DOI 10.1016/0370-2693(84)90490-8
83. K. Nagai, et al., Phys. Lett. **B278**, 506 (1992). DOI 10.1016/0370-2693(92)90593-S
84. K. Okabe, et al., Phys. Lett. **B423**, 407 (1998). DOI 10.1016/S0370-2693(98)00073-2
85. B.A. Schumm, et al., Phys. Rev. **D46**, 453 (1992). DOI 10.1103/PhysRevD.46.453
86. P. Abreu, et al., Phys. Lett. **B347**, 447 (1995). DOI 10.1016/0370-2693(95)00190-V
87. R. Akers, et al., Phys. Lett. **B352**, 176 (1995). DOI 10.1016/0370-2693(95)00510-R
88. P. Abreu, A. De Angelis, DELPHI NOTE **2002-052**, CONF 586 (2002)
89. Yu. Dokshitzer, F. Fabbri, V.A. Khoze, W. Ochs, Eur. Phys. J. **C45**, 387 (2006). DOI 10.1140/epjc/s2005-02424-5
90. A.J. Larkoski, J. Thaler, W.J. Waalewijn, JHEP **11**, 129 (2014). DOI 10.1007/JHEP11(2014)129
91. J. Mo, F.J. Tackmann, W.J. Waalewijn, (2017)
92. J. Bellm, G. Nail, S. Plätzer, P. Schichtel, A. Siódmok, Eur. Phys. J. **C76**(12), 665 (2016). DOI 10.1140/epjc/s10052-016-4506-x
93. J. Bellm, S. Plätzer, P. Richardson, A. Siódmok, S. Webster, Phys. Rev. **D94**(3), 034028 (2016). DOI 10.1103/PhysRevD.94.034028

94. S. Mrenna, P. Skands, Phys. Rev. **D94**(7), 074005 (2016). DOI 10.1103/PhysRevD.94.074005 s10052-016-4430-0
95. E. Bothmann, M. Schönherr, S. Schumann, Eur. Phys. J. **C76**(11), 590 (2016). DOI 10.1140/epjc/